DOI: 10.19884/j.1672-5220.202403009

Design of Low-Frequency Vibration Isolation System for On-Board Inertial Navigation System in Agricultural Vehicles

ZHOU Yang, CHEN Cheng, SUN Zhihong *
College of Mechanical Engineering, Donghua University, Shanghai 201620, China

Abstract: A small quasi-zero stiffness (QZS) vibration isolator is designed to be mounted on the roof of an agricultural vehicle for the working environment and vibration frequency of the inertial navigation system. By using the principle that the Euler beam has a negative stiffness in the critical state, the dynamic stiffness of the loaded QZS vibration isolator in the balance position tends to be close to zero by connecting a vertical spring in parallel. Firstly, the stiffness of the QZS vibration isolation system at the balance position is analyzed statically, and the material parameters and properties of the Euler beam are determined. Then, the dynamic equations are established, and the harmonic equilibrium method is used to solve the dynamic response under sinusoidal excitation to obtain the force transmissibility of the QZS vibration isolation system, and to make a comparison with that of the linear isolation system. Finally, the modal simulation, harmonic response simulation and random vibration simulation of the QZS vibration isolator are carried out through the finite element analysis, and the results show that the QZS vibration isolator has a lower initial isolation frequency and a larger isolation range, and the peak vibration isolation can reach about 11.58 dB.

Keywords: vibration isolator; quasi-zero stiffness (QZS); buckling; Euler beam; finite element analysis
CLC number: OB28 **Document code**: A
Article ID: 1672-5220(2025)01-0054-10

Open Science Identity (OSID)

0 Introduction

Driving agricultural vehicles on unpaved roads produces unavoidable vibrations, and these vibrations have a certain impact on the normal operation of the vehicles[1]. Nowadays, unmanned technology is developing rapidly, and the key technology of unmanned agricultural vehicles is the inertial navigation system[2-3]. However, the vibration generated by the road surface excitation has an impact on the normal operation of the inertial navigation system. Especially, the frequency vibrations of 50 Hz or less have a greater impact on the inertial navigation system.

A lot of research has been done on the vibration reduction of the inertial navigation system at home and abroad. The French company Ixblue has designed a small and high-precision inertial-guided vibration isolation structure that effectively insulated against external vibrations[4]. Researchers from Russia and Ukraine have used jitter-optimized configurations to solve the jitter coupling of the system and improve the dynamic accuracy[5]. Honeywell has learned from several successful vibration isolation systems the key design points for designing the right geometry and dimensions for the vibration isolation system[6]. Yao[7] proposed six damping modes for an inertial navigation system and provided a reference for the research of the damping mechanism. Based on the finite element method, Gao et al.[8] quantitatively analyzed the inertial navigation system installed with vibration isolators through a software, which provided an important reference for the optimization of vibration isolators. Wang[9] designed the vibration isolation device of the inertial navigation system for the vehicle fiber-optic-gyroscope strapdown inertial navigation system. Tu et al.[10] designed a fluoro-silicone rubber damper for the inertial navigation system and analyzed its dynamic characteristics. Current research primarily focuses on isolating high-frequency vibrations in the inertial navigation system[11], with isolators mainly based on the principle of passive isolation. This principle does not apply to isolating low-frequency vibrations. The research method in Ref. [12] employed therein is worth considering.

In low-frequency vibration isolation, the quasi-zero stiffness (QZS) principle is commonly employed. This principle involves connecting a negative stiffness mechanism[13] with a positive stiffness mechanism in parallel. As a result, the total dynamic stiffness of the vibration isolation system at the equilibrium points approaches zero. In the balance position, the load-bearing capacity of the vibration isolation system is provided by the positive stiffness mechanism. This process enables the system to have a favorable load-carrying capacity with low-frequency vibration isolation. The most common type of the QZS vibration isolation is

Received date: 2024-03-19
* Correspondence should be addressed to SUN Zhihong, email: zhsun@dhu.edu.cn
Citation: ZHOU Y, CHEN C, SUN Z H. Design of low-frequency vibration isolation system for on-board inertial navigation system in agricultural vehicles[J]. *Journal of Donghua University (English Edition)*, 2025, 42(1): 54-63.

the mechanical spring structure[14]. The structure uses the negative stiffness generated by the two inclined springs to offset the positive stiffness of the vertical spring, but the overall structure occupies a larger area. Zhou et al.[15] proposed a geometrically nonlinear structure, and the structure of the system consisted of a cam-roller-spring. The vibration isolation effect of the system is better when the value of excitation amplitude is higher. Jiang et al.[16] used a magnetic structure to provide negative stiffnesses, and the vibration isolation system was formed with good vibration isolation in all six degrees of freedom directions. Dai et al.[17] proposed a bionic structure similar to a kangaroo leg, and the QZS vibration isolation system composed of this structure was compact and bulky.

Since the vibration isolator of the inertial navigation system in this study is mounted on the roof of the vehicle, the installation space of the vibration isolator is small and the structure must not be too complicated. Therefore, it is necessary to design a low-frequency vibration isolator with a small size and a simple structure. In this paper, the principle that the Euler beam has a negative stiffness in flexure is used for the first time to design low-frequency vibration isolators[18] in the vibration isolation of on-board electronic equipment for agricultural vehicles. The intrinsic frequency of the overall system might be reduced, and the overall system might have a good load-bearing capacity. The parameters of the QZS vibration isolator in the balance position are determined by static analyses. Then the modal simulation of the QZS vibration isolator is carried out by the finite element analysis[19-21] to verify that the QZS vibration isolation system has a low intrinsic frequency, and the harmonic response simulation and random vibration simulation are carried out to verify whether the QZS vibration isolator has a better vibration isolation effect in the low-frequency range.

1 Static Analyses

Euler beams are used as the negative stiffness members of the QZS vibration isolation system. The Euler beam[22-23] provides a negative stiffness to the QZS vibration isolation system when it is flexed, and cancels out the positive stiffness provided by the parallel vertical springs in the balance position, making the dynamic stiffness of the vibration isolation system zero. Figure 1 shows that the Euler beam hinged at both ends is subjected to an axial force P. Assuming that the vertical displacement of the center point of the Euler beam from the axis at the initial position is y (y_0 corresponds to the initial defect of the buckling beam), and the displacement in the direction of the axis is x, then the expression for P[24] is

$$P = P_e - \left\{1 - \pi^2\left(\frac{y}{L}\right)^2\left[\pi^2\left(\frac{y}{L}\right)^2 + 4\left(\frac{x}{L}\right)\right]^{-\frac{1}{2}}\right\} \times \left[1 + \frac{\pi^2}{8}\left(\frac{y}{L}\right)^2 + \frac{1}{2}\left(\frac{x}{L}\right)\right], \tag{1}$$

where L is the length of the Euler beam; P_e is the first-order critical buckling strength, $P_e = EI(\pi/L)^2$, E is the elastic modulus of the material and I is the sectional moment of inertia of the beam.

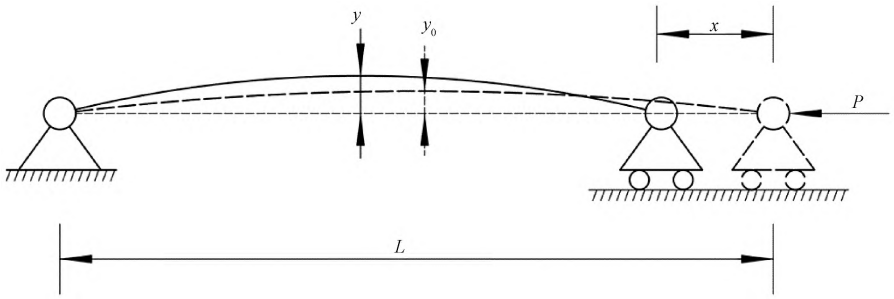

Fig. 1 Euler beam hinged at both ends subjected to axial force

Figure 2 shows that the system is subjected to a vertical displacement by the vertical force F at the initial position, the Euler beam rotates by an angle β, and u is the vertical displacement.

$$F = P_e\left\{1 - \pi\left(\frac{y}{L}\right)\left[\pi^2\left(\frac{y}{L}\right)^2 + 4\left(\frac{x}{L}\right)\right]^{-\frac{1}{2}}\right\} \times \left[1 + \frac{\pi^2}{8}\left(\frac{y}{L}\right)^2 + \frac{1}{2}\left(\frac{x}{L}\right)\right]\sin\beta, \tag{2}$$

where

$$\begin{cases} \dfrac{x}{L} = 1 - \sqrt{1 + \left(\dfrac{z}{L}\right)^2 - 2\left(\dfrac{z}{L}\right)\sin\alpha}, \\ \sin\beta = \dfrac{L\sin\alpha - z}{\sqrt{L^2 + z^2 - 2Lz\sin\alpha}}, \end{cases} \tag{3}$$

α is the tilt angle, and z is the displacement of the Euler beam under compression.

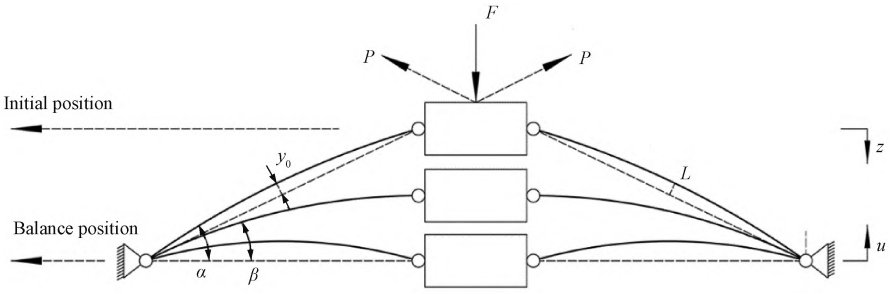

Fig. 2 Force analysis diagram of inclined Euler beam

In the balance position, changing the coordinate system, let $u = z - L\sin\alpha$ and $\delta = \cos\alpha$, which gives

$$\frac{x}{L} = 1 - \sqrt{1 + \left(\frac{u}{L}\right)^2 - (\sin\alpha)^2}. \tag{4}$$

Substitute Eqs. (3) and (4) into Eq. (2), and non-dimensionalize them:

$$\tilde{F} = \lambda\left\{1 - \pi\tilde{Y}\left[(\pi\tilde{Y})^2 + 4\left(1 - \sqrt{\tilde{U}^2 + \delta^2}\right)\right]^{-\frac{1}{2}}\right\} \times \left[1 + \frac{(\pi\tilde{Y})^2}{8} + \frac{1}{2}\left(1 - \sqrt{\tilde{U}^2 + \delta^2}\right)\right]\left(\frac{-u}{\sqrt{L^2 + \tilde{U}^2}}\right), \tag{5}$$

where $\tilde{F}$ is a dimensionless force, $\tilde{F} = \frac{F}{kL}$, and k is the stiffness coefficient; λ is the dimensionless stiffness ratio and $\lambda = \frac{P_e}{kL}$; $\tilde{Y} = \frac{y}{L}$; $\tilde{U} = \frac{u}{L}$.

Based on the definition of the stiffness, the dimensionless stiffness of the system is obtained from the derivation of the dimensionless displacement:

$$\tilde{k}_d = \left\{\frac{2\lambda\pi\tilde{Y}\left[3 + (\pi\tilde{Y})^2/4 - \sqrt{\delta^2 + \tilde{U}^2}\right]}{[\delta^2 + \tilde{U}^2]\left[(\pi\tilde{Y})^2 + 4 - 4\sqrt{\delta^2 + \tilde{U}^2}\right]^{\frac{3}{2}}}\right\} + \left\{\frac{\sqrt{(\pi\tilde{Y})^2 + 4 - 4\sqrt{\delta^2 + \tilde{U}^2}} - \pi\tilde{Y}}{(\pi\tilde{Y})^2 + 4 - 4\sqrt{\delta^2 + \tilde{U}^2}}\right\} \times \left\{1 + \frac{\delta^2[3 + (\pi\tilde{Y})^2/4]}{(\delta^2 + \tilde{U}^2)^{\frac{3}{2}}}\right\}. \tag{6}$$

Figure 3 shows the schematic structure of a QZS vibration isolator (an Euler beam as a negative stiffness mechanism). Two oblique Euler beams are fixed after one section, and the other end is hinged with the load-bearing block. The load-bearing block is connected in parallel with a vertical spring. k_1 and c are the stiffness coefficient and the damping coefficient of the vertical spring, respectively.

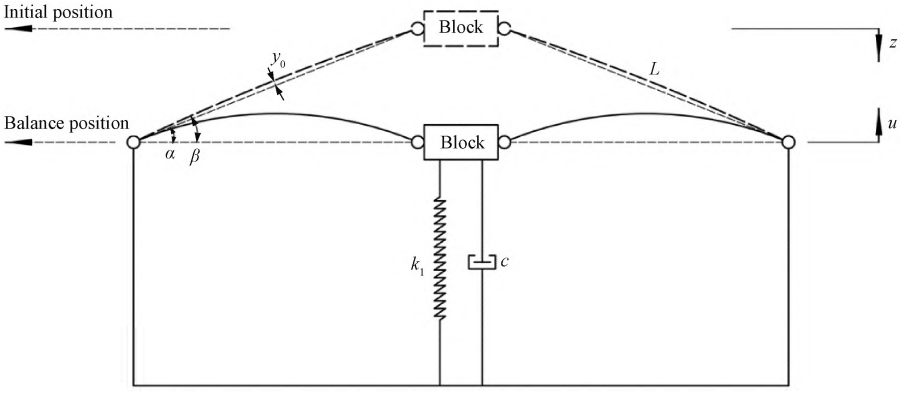

Fig. 3 Schematic structure of QZS vibration isolator

The vibration isolation system is pressed down to the balance position under the gravity of the load-bearing block. Currently, the return force of the vibration isolation system in the vertical direction F_v consists of the return force of the Euler beam F_d and the return force of the parallel connected vertical spring F_1.

$$F_V = F_d + F_1 = F_d + k_1(u + L\sqrt{1 - \delta^2}). \tag{7}$$

The dimensionless form of Eq. (7) is

$$\tilde{F}_V = n\lambda\left\{1 - \pi\tilde{Y}\left[\pi^2\tilde{Y}^2 + 4\left(1 - \sqrt{\tilde{U}^2 + \delta^2}\right)\right]^{-\frac{1}{2}}\right\} \times \left[1 + \frac{\pi^2\tilde{Y}^2}{8} + \frac{1}{2}\left(1 - \sqrt{\tilde{U}^2 + \delta^2}\right)\right]\left(\frac{-u}{\sqrt{L^2 + \tilde{U}^2}}\right) - \left(\tilde{U} + \sqrt{1 - \delta^2}\right), \tag{8}$$

where $\tilde{F}_V$ is a dimensionless return force and $\tilde{F}_V = \frac{F}{k_1 L}$; n is the number of Euler beams.

Then the dimensionless stiffness of the whole $\tilde{k}_V$ is

$$\tilde{k}_V = \left\{ \frac{2n\lambda\pi\tilde{Y}\tilde{U}\left[3+(\pi\tilde{Y})^2/4-\sqrt{\delta^2+\tilde{U}^2}\right]}{[\delta^2+\tilde{U}^2]\left[(\pi\tilde{Y})^2+4-4\sqrt{\delta^2+\tilde{U}^2}\right]^{\frac{3}{2}}} \right\} + 1 + \lambda n \left\{ \frac{\sqrt{(\pi\tilde{Y})^2+4-4\sqrt{\delta^2+\tilde{U}^2}}-\pi\tilde{Y}}{\sqrt{(\pi\tilde{Y})^2+4-4\sqrt{\delta^2+\tilde{U}^2}}} \right\} \left\{ 1+\frac{\delta^2[3+(\pi\tilde{Y})^2/4]}{(\delta^2+\tilde{U}^2)^{\frac{3}{2}}} \right\}. \quad (9)$$

When $\tilde{U} = 0$, the vibration isolation system is in a balance position, let $\tilde{k}_V = 0$, and λ can be obtained:

$$\lambda = -\frac{1}{n\left[1-\pi\tilde{Y}/\sqrt{(\pi\tilde{Y})^2+4-4\delta}\right]\left\{1-\frac{1}{\delta}[3+(\pi\tilde{Y})^2/4]\right\}}. \quad (10)$$

The dimensionless force-displacement and the stiffness-displacement curve of the QZS vibration isolation system can be obtained by substituting Eq. (10) into Eqs. (8) and (9), as shown in Figs. 4 and 5, respectively.

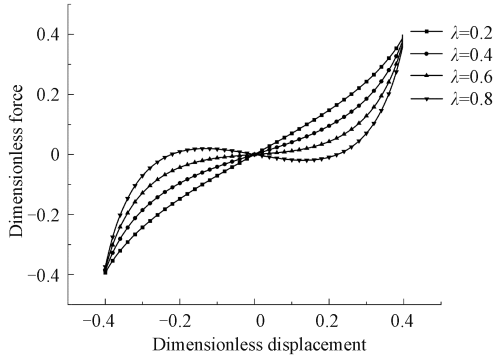

Fig. 4 Dimensionless force-displacement curves

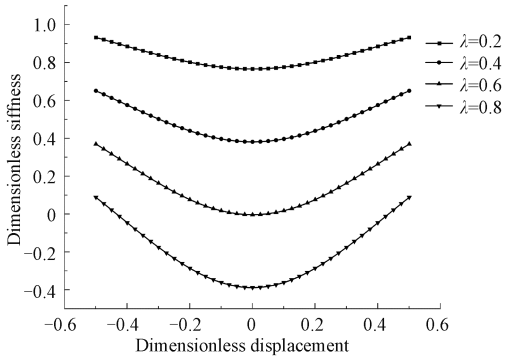

Fig. 5 Dimensionless stiffness-displacement curves

For the installation stability of the system, n is set to be 4, and from Ref. [18], $\tilde{Y} = 3\%$. From Fig. 5, it can be seen that when λ increases, the dimensionless stiffness of the system decreases, and the dimensionless force undulates more with the dimensionless displacement. When $\lambda = 0.4$, the dimensionless force-displacement curve is more gentle, and can be closer to the equilibrium position ($\tilde{U} = 0$), so that the dimensionless stiffness $\tilde{k}_V \approx 0$. Substituting $\lambda = 0.4$ and $\tilde{Y} = 3\%$, it can be found that the tilt angle of the Euler beam is about 25°.

$$\lambda = \frac{P_e}{k_1 L} = \frac{EI\pi^2}{k_1 L^3}. \quad (11)$$

Equation (11) is the specific expression for λ. The gravity of the QZS vibration isolation system is 20 N. In the balance position, the load-bearing capacity of the QZS vibration isolation system is provided by the vertical spring, and the stiffness coefficient of the vertical spring is

$$k_1 = \frac{mg}{L\sqrt{1-\delta^2}} \approx 0.788\ 7\ \text{N/m}. \quad (12)$$

The moment of inertia of the cross-section of the Euler beam[25] is

$$I = \frac{bh^3}{12}, \quad (13)$$

where b is the width of the cross-section; h is the height of the cross-section.

Substituting Eq. (13) into Eq. (11) gives:

$$\lambda = \frac{E\pi bh^3}{12k_1 L^3}. \quad (14)$$

It can be seen from Eq. (14) that λ increases with b and h, as shown in Fig. 6.

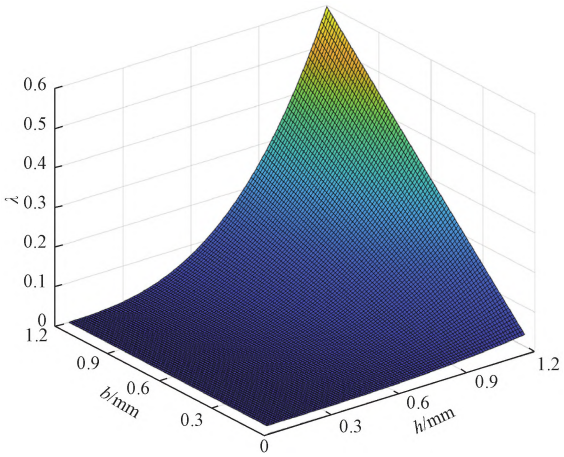

Fig. 6 Stiffness ratio vs. cross-section size

The stiffness ratio can be determined by the size of the Euler beam as well as the material. First of all, the Euler beam needs to have a good bending fatigue resistance and a good elastic limit. The 65Mn material could meet the requirements.

By calculation, suitable material parameters are selected as shown in Table 1.

Table 1 Euler beam material parameters

Material	L/mm	b/mm	h/mm	E/GPa	α/(°)
65Mn	60	2	1	206	25

Based on the above parameters, the prototype model of the QZS vibration isolator is established as shown in Fig. 7. The QZS vibration isolator mainly consists of the Euler beams, a load-bearing block, load-bearing columns, vertical linear springs and a foundation. The Euler beams are symmetrically connected to the four directions of the load-bearing block, the other end is connected to the load-bearing columns which are fixed in the four mounting holes of the foundation, and a vertical linear spring is placed between the load-bearing block and the foundation.

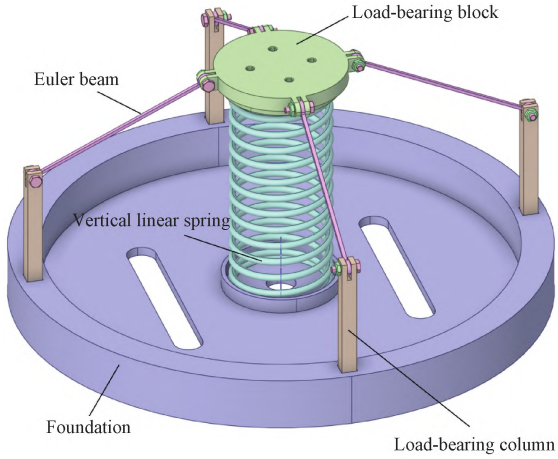

Fig. 7 QZS vibration isolator prototype model

2 Dynamic Analyses

The very complex expression for the return force of the QZS vibration isolator is obtained by approximating the 5th-order expansion of Eq. (8) using a Taylor expansion[22,26]:

$$f = \sum_{n=1}^{N} \sigma_{2n+1} \tilde{u}^{2n+1}, \tag{15}$$

where f is an approximation of the Taylor's unfolded return force; σ is the coefficient of the quadratic term after the Taylor expansion; $\tilde{u}$ is the approximate dimensionless displacement after Taylor expansion.

When the overall mass of the QZS vibration isolation system m is loaded onto the QZS vibration isolator, one end of the Euler beam is displaced by the force, and the QZS vibration isolation system is in the balance position at this time. Let the damping at this time is linear. The excitation of the system is sinusoidal, and the equation of the system motion can be obtained at this time:

$$m\ddot{u} + c\dot{u} + k_1 L\Big(\sum_{n=1}^{N} \sigma_{2n+1} \tilde{u}^{2n+1} + \sqrt{1-\delta^2}\Big) - mg = A\cos(\omega t), \tag{16}$$

where A is the amplitude; c is the damping factor; ω is the angular frequency.

Introduce dimensionless parameters:

$$\omega_n = \sqrt{\frac{k_1}{m}},\ \Omega = \frac{\omega}{\omega_n},\ \tau = \omega_n t,\ \xi = \frac{c}{2m\omega_n},\ f_0 = \frac{A}{\omega_n^2 mL},$$

where ω_n is the natural frequency; Ω is the frequency ratio; τ is the number of vibrations per unit time; ξ is the damping ratio; f_0 is the amplitude ratio. Taking these dimensionless parameters into Eq. (16), the differential equation of motion is obtained after non-dimensionalization:

$$\ddot{\tilde{u}} + 2\xi\dot{\tilde{u}} + \sum_{n=1}^{N} \sigma_{2n+1} \tilde{u}^{2n+1} = A\cos(\Omega\tau). \tag{17}$$

When the QZS vibration isolation system is in the balance position, the support force will be completely provided by the vertical linear spring. Removing the Euler beam structure, there is no system displacement in the vertical direction. The system at this time is equivalent to a linear vibration isolation system, the differential equation of motion of the equivalent linear vibration isolation system is

$$\ddot{\tilde{u}} + 2\xi\dot{\tilde{u}} + \tilde{u} = A\cos(\Omega\tau). \tag{18}$$

Equation (18) is solved by the harmonic balance method, and finally, the force transmissibility of the QZS vibration isolator T_f can be obtained:

$$T_f = \sqrt{\Big(\sum_{n=1}^{N} \sigma_{2n+} \delta_0^{2n+1}\Big)^2 + (2\xi\Omega\delta_0)^2}/A, \tag{19}$$

where δ_0 is an approximation of the dimensionless vertical displacement.

The equivalent linear vibration isolation system has a force transmissibility:

$$T_f' = \sqrt{\frac{1 + 4\xi^2\Omega^2}{(1-\Omega^2)^2 + 4\xi^2\Omega^2}}. \tag{20}$$

Figure 8 shows the force transmissibility curves of the QZS vibration isolator and the linear isolator. The QZS vibration isolator has a lower initial isolation frequency, and the initial isolation frequency can be infinitely close to zero theoretically. It is a great advantage compared to the linear isolator that cannot

isolate the vibration when the isolation frequency is less than the intrinsic frequency. The QZS vibration isolator can broaden the frequency of isolation. At the same time, as the excitation amplitude decreases, the peak force transmissibility of the QZS vibration isolator also decreases. Thus, the smaller the excitation amplitude of the scenario, the more obvious the isolation effect of the QZS vibration isolator.

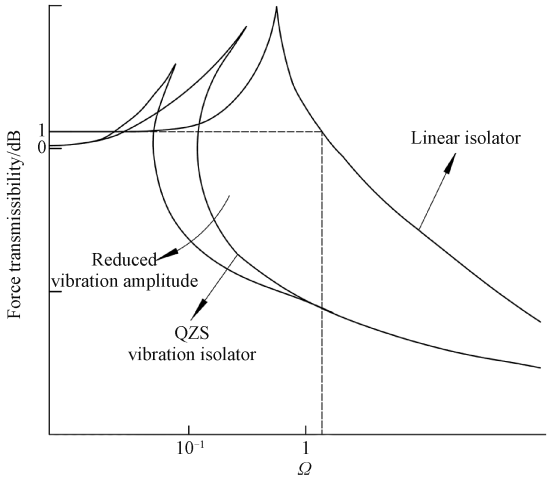

Fig. 8 Force transmissibility

3 Finite Element Analyses

3.1 Buckling analyses

Based on the SolidWorks software, the finite element model of the Euler beam is established (L = 60 mm, h = 1 mm, b = 2 mm, and E = 206 GPa). Through the eigenvalue buckling analysis of the workbench, a section of the beam is fixedly supported and an axial load of 1 N is applied at the other end. The eigenvalue buckling analysis is performed to obtain the critical load at which the Euler beam reaches the buckling state. The simulation analyzes the first two orders of vibration patterns. In the first order of yielding vibration patterns as shown in Fig. 9, the flexural deformation occurs in the middle position of the Euler beam, and the yield load is 24.94 N. In the second order of yielding vibration patterns as shown in Fig. 10, the flexural deformation occurs in the positions of 1/4 length from the two ends, and the yield load is 61.98 N.

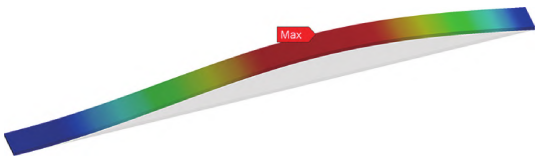

Fig. 9 Deformation under first-order flexural strength

Fig. 10 Deformation under second-order flexural strength

Before the modal analysis of the vibration isolator, a static analysis is carried out. The model is simplified to a certain extent, the vertical linear spring is replaced by the spring connection element in the software, the fixed support is applied to the base of the vibration isolator, and the pre-stressing is applied to the intermediate load-bearing parts to simulate the gravitational force exerted by the vibration-isolated system on the vibration isolator. Figure 11 shows the deformation of the QZS vibration isolation system under pre-stressing, and it can be seen that the isolator is in the balance position. Figure 12 shows the equivalent stress cloud diagram in the balance position, the maximum stress point of the Euler beam is at 1/2 of the Euler beam, which is 102.2 MPa. According to the buckling analysis of the Euler beam, the yield load of the first section is 24.94 N, and it can be calculated that the yield strength is about 99.8 MPa, and the Euler beam is in the state of buckling when it is in the balance position.

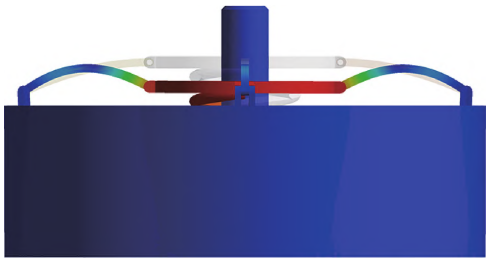

Fig. 11 Deformation cloud under pre-stressing

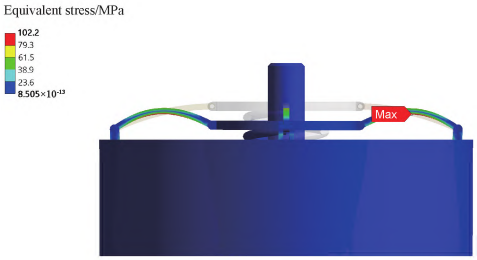

Fig. 12 Stress cloud under pre-stressing

3.2 Modal analyses

With the results obtained from the static analyses, the solution is linked to the modal analyses, and the first six orders of modes are analyzed by applying a fixed support to the base of the QZS vibration isolator.

The main vibration mode is the vibration in the vertical direction as shown in Fig. 13 (d), which is the vibration mode that we want to focus on. The intrinsic frequency is 4.3091 Hz, which is in a small range. Since the external excitation of the vehicle-mounted inertial

navigation system is mainly the vibration excitation in the vertical direction from 0 to 50 Hz, the QZS vibration isolator has a low initial isolation frequency in the vertical direction.

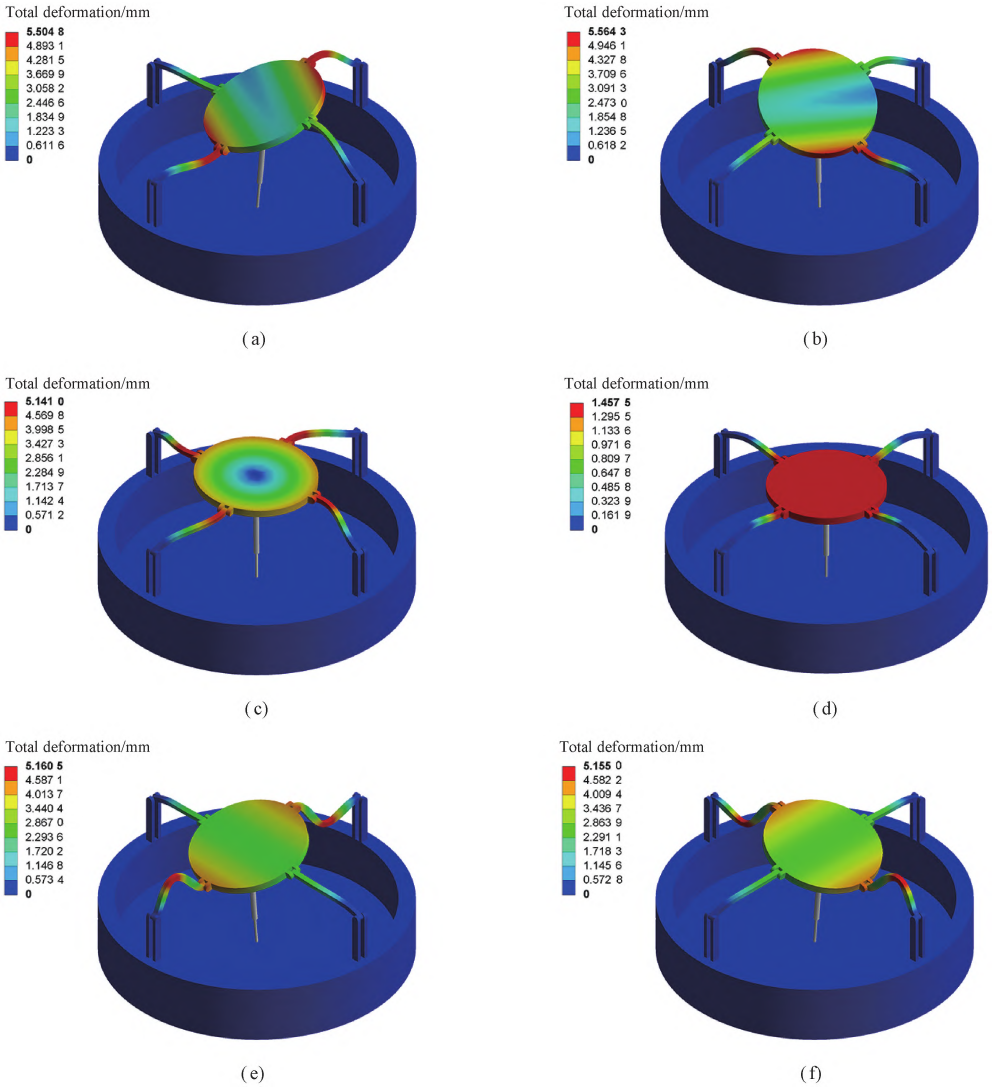

Fig. 13 Results of modal analyses: (a) first-order intrinsic frequency (9.177 7 Hz); (b) second-order intrinsic frequency (9.180 6 Hz); (c) third-order intrinsic frequency (9.256 8 Hz); (d) fourth-order intrinsic frequency (4.309 1 Hz); (e) fifth-order intrinsic frequency (30.054 0 Hz); (f) sixth-order intrinsic frequency (30.079 0 Hz)

3.3 Harmonic response analyses

Through the harmonic response analyses of the QZS vibration isolator sweeping action, the dynamic response of the QZS vibration isolator in the external sinusoidal excitation is obtained, and the amplification effect on the structural safety of the QZS vibration isolation system is determined. In industrial design, when the driving environment of ground vehicles is 5M4, it is necessary to perform the frequency sweep analysis on the onboard electronic equipment. Therefore, according to the national standard GB/T 4798.5—2007, the harmonic response analysis is carried out on the QZS isolator structure. Two sinusoidal excitations are inserted in the analysis setup: an acceleration amplitude of 2 mm/s^2 and a displacement amplitude of 7.5 mm. The position for adding the load is on the base of the isolator, and its direction is vertical. The specific input settings are shown in Table 2.

Table 2 Steady-state sinusoidal excitation

Frequency range/Hz	Acceleration amplitude/(mm/s^2)	Displacement amplitude/mm
[2, 8]	2	0
(8, 50]	0	7.5

The frequency response is shown in Fig. 14. The response amplitude is higher at the point where the main intrinsic frequency vibration pattern is the intrinsic frequency in the vertical direction. This indicates that there is a frequency amplification point in the QZS vibration isolator. In the rest of the frequency range, the

acceleration amplitude is reduced to less than 1 mm/s^2, indicating the excellent vibration isolation capability of the QZS vibration isolator.

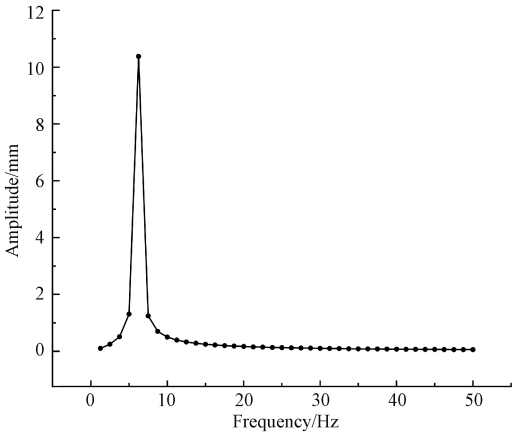

Fig. 14 Amplitude-frequency diagram of harmonic response analysis

3.4 Random vibration analyses

As shown in Fig. 15, the connection between the QZS vibration isolator and the inertial navigation system is made by using bolts and nuts. The QZS vibration isolators are placed in all four directions of the inertial navigation system to increase the stability of the overall vibration isolation system. The characteristic bolt and nut features and the small feature curves on the inertial navigation system cover are simplified in the simulation to reduce the defects in the mesh delineation. The bottom of the QZS vibration isolator is fixedly supported.

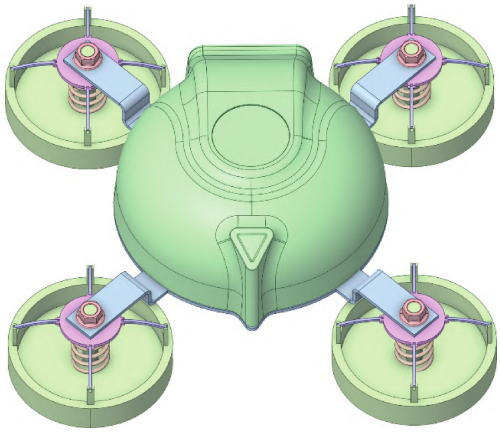

Fig. 15 Schematic diagram of QZS vibration isolation system

Figure 16 shows the random vibration signal measured at the center of the rigidly connected inertial navigation system when the agricultural vehicle travels at 8 km/h. The time-domain signal of the vibration is converted into the displacement power spectral density. The displacement power spectral density is loaded onto a fixed support and the probe is added to the center of the inertial navigation system for response signal acquisition.

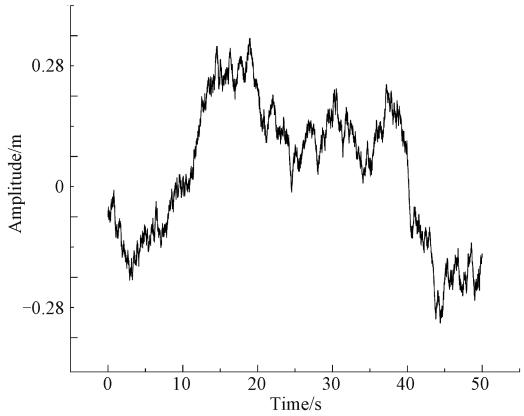

Fig. 16 Vibration time-domain signals of agricultural vehicle traveling at 8 km/h

As shown in Fig. 17, after vibration isolation, the center point vibration response of the system decreases significantly compared to that before vibration isolation. As can be seen in Table 3, the maximum vibration isolation is achieved at the peak of vibration from 0−10 Hz with a reduction of approximately 11.58 dB, and the amount of vibration isolation decreases when the frequency is higher than 10 Hz. This is consistent with the results of the dynamic analysis in Section 2, where the force transmissibility of the QZS vibration isolation system decreases with the increase of the excitation amplitude. At the same time, the vibration response is amplified at the point of the intrinsic frequency of the vertical vibration, which is consistent with the conclusion from the harmonic response analysis that the overall isolation efficiency is higher than that of the direct rigid connection.

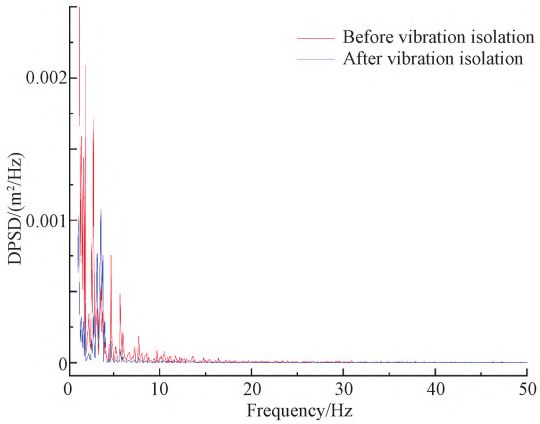

DPSD—displacement power spectral density.

Fig. 17 Comparison of DPSD before and after vibration isolation

Table 3 Average DPSD before and after vibration isolation

Frequency/Hz	Average DPSD/(m^2/Hz)		Vibration isolation capacity/dB
	Before isolation	After isolation	
[0, 10)	1.563×10^{-3}	4.12×10^{-4}	11.58
[10, 30)	1.32×10^{-4}	7.4×10^{-5}	5.00
[30, 520]	6.4×10^{-5}	3.5×10^{-5}	5.24

4 Conclusions

In this paper, a QZS vibration isolator is designed for the onboard inertial navigation system of agricultural vehicles based on the principle that the Euler beam has a negative stiffness during the flexed state. The relationship between the parameters of the QZS vibration isolation system and the stiffness characteristics in the balance position is analyzed through theoretical calculation, and the specific structural dimensions and material parameters of the required Euler beam are obtained. The force transmissibility of the QZS vibration isolator is obtained through kinetic calculation, and compared with that of the linear isolator, it is concluded that the QZS vibration isolator has a lower initial isolation frequency than the equivalent linear isolator. The QZS vibration isolator has a greater advantage in low-frequency vibration isolation. The modal simulation of the QZS vibration isolator is carried out through finite element analysis. The QZS vibration isolator has a low intrinsic frequency, especially in the vertical vibration mode, and its intrinsic frequency is the lowest, which indicates that the QZS vibration isolation system has a low initial vibration isolation frequency. The harmonic response analysis shows that the QZS vibration isolation system has a certain vibration isolation ability at the resonant frequency, but the frequency amplification still occurs in the position of its intrinsic frequency. Random vibration simulation further verifies that the designed QZS vibration isolator has a low initial vibration isolation frequency, a high vibration isolation efficiency in the low-frequency range, and a peak vibration suppression of about 11.58 dB, which can effectively reduce the vibration excitation from the outside world.

References

[1] YUAN J Q, ZHOU Y Q, FAN J, et al. Research on vibration characteristics of tractor driving on the farmland [J]. *Journal of Chinese Agricultural Mechanization*, 2020, 41(2): 127-134. (in Chinese)

[2] XU G F, CHEN M Z, JIN C Q, et al. A review of key technology of tractor automatic driving[J]. *Journal of Chinese Agricultural Mechanization*, 2022, 43(6): 126-134. (in Chinese)

[3] JI X, WANG S R. Adaptive design for vibration environment of electronic equipment [M]. Beijing: Publishing House of Electronics Industry, 2012. (in Chinese)

[4] BRAMAN T, GROSSMAN O. Designing vibration and shock isolation systems for micro electrical machined based inertial measurement units[C]//2006 IEEE/ION Position, Location, and Navigation Symposium. Coronado, USA: IEEE, 2006: 400-404.

[5] LAHHAM J I, WIGENT D J, COLEMAN A L. Tuned support structure for structure-borne noise reduction of inertial navigator with dithered ring laser gyros (RLG) [C]//IEEE 2000 Position Location and Navigation Symposium. San Diego, USA: IEEE, 2000: 419-428.

[6] BANERJEE K, DAM B, MAJUMDAR K, et al. An improved dither-stripping scheme for strapdown ring laser gyroscopes[C]//2004 IEEE Region 10 Conference TENCON 2004. Chiang Mai, Thailand: IEEE, 2004: 689-692.

[7] YAO J J. Contrast of different vibration isolation patterns used in strap-down inertial navigation system [J]. *Structure & Environment Engineering*, 2009, 36(2): 19-27.

[8] GAO J Q, TANG X Q, HUANG X Y, et al. FEA method for analysis of SINS error caused by vibration isolation system [J]. *Acta Armamentarii*, 2016, 37(9): 1570-1577.

[9] WANG D C. Optimal design of vehicle FOG strapdown inertial navigation system [D]. Harbin: Harbin Engineering University, 2021. (in Chinese)

[10] TU C C, CHEN Z A, ZHANG X S, et al. Vibration performance of fluoro-silicone rubber vibration absorber for inertial navigation [J]. *Ordnance Material Science and Engineering*, 2023, 46(5): 131-136. (in Chinese)

[11] DUAN Z Y, CHU H R, JIA H G, et al. Researches on designing of MEMS strapdown inertial navigation vibration damping system [J]. *Journal of Mechanical Strength*, 2017, 39(4): 797-803. (in Chinese)

[12] YI X B, SHENG X W, XU Y, et al. Characteristic analysis and harmonic feature identification of micro-vibration on flywheels [J]. *Journal of Donghua University (English Edition)*, 2021, 38(1): 28-35.

[13] PENG X, CHEN S N, SONG F P. Research on theory of negative stiffness and its application [J]. *Journal of Hunan University (Natural Sciences)*, 1992(4): 89-94. (in Chinese)

[14] MENG L S, SUN J G, FU N, et al. Design and analysis of a novel quasi-zero stiffness vibration isolation system [J]. *Journal of Vibration and Shock*, 2014, 33(11): 195-199. (in Chinese)

[15] ZHOU J X, WANG X L, XU D L, et al. Experimental study on vibration isolation characteristics of the quasi zero stiffness isolator with camroller mechanism [J]. *Journal of Vibration Engineering*, 2015, 28(3): 449-455. (in Chinese)

[16] JIANG Y L, SONG C S, DING C M, et al. Design of magnetic-air hybrid quasi-zero stiffness vibration isolation system[J]. *Journal of Sound and Vibration*, 2020, 477: 115346.

[17] DAI H H, JING X J, WANG Y, et al. Post-capture vibration suppression of spacecraft via a

bio-inspired isolation system [J]. *Mechanical Systems and Signal Processing*, 2018, 105: 214-240.
[18] HUANG X C, LIU X T, SUN J Y, et al. Vibration isolation characteristics of a nonlinear isolator using Euler buckled beam as negative stiffness corrector: a theoretical and experimental study [J]. *Journal of Sound and Vibration*, 2014, 333(4): 1132-1148.
[19] LIU R F, ZHANG H J. Static load and modal analysis of electronic cabinet based on finite element method [J]. *Electro-Mechanical Engineering*, 2014, 30(1): 11-13, 51. (in Chinese)
[20] YANG W F, WEI Q, ZHU L Q. Anti-vibration design for an airborne electronic equipment based on finite element method [J]. *Journal of Vibration and Shock*, 2010, 29(5): 230-234, 253. (in Chinese)
[21] ZHANG J D, LIU H B. The modal analysis of airborne equipment bracket based on ANSYS [J]. *Journal of Xihua University (Natural Science Edition)*, 2012, 31(2): 54-57. (in Chinese)
[22] LIU X T, SUN J Y, XIAO F, et al. Principle and performance of a quasi-zero stiffness isolator for micro-vibration isolation [J]. *Journal of Vibration and Shock*, 2013, 32(21): 69-73. (in Chinese)
[23] YAN J. Characterization analysis of quasi-zero-stiffness isolator and application on satellite vibration suppression [D]. Harbin: Harbin Engineering University, 2016. (in Chinese)
[24] VIRGIN L N, DAVIS R B. Vibration isolation using buckled struts [J]. *Journal of Sound and Vibration*, 2003, 260(5): 965-973.
[25] PAN Y, ZHAO T. Discussion on the method of solving the moment of inertia of cross-section of common engineering components [J]. *China Science and Technology Information*, 2012(10): 90. (in Chinese)
[26] LIU X T, HUANG X C, ZHANG Z Y, et al. Influence of excitation amplitude and load on the characteristics of quasi-zero stiffness isolator [J]. *Journal of Mechanical Engineering*, 2013, 49(6): 89-94. (in Chinese)

农用车辆车载惯导系统的低频隔振系统设计

周　阳，陈　成，孙志宏*
东华大学 机械工程学院，上海 201620

摘　要：针对农用车辆在复杂工作环境下惯导系统的稳定性问题，设计了一种小型车顶安装式准零刚度隔振器：利用欧拉梁在临界状态时具有负刚度特性的原理，通过欧拉梁与竖直弹簧的并联，使得加载后的准零刚度隔振器在平衡位置的动刚度趋近于零。首先，通过对平衡位置时准零刚度隔振系统的刚度特性进行静力学分析，确定欧拉梁的材料参数和材料属性；其次，建立动力学方程，并采用谐波平衡法，求解在正弦激励下的动力学响应，获得其力传递率，并与线性隔振系统的力传递率进行对比；最后，通过有限元分析，对准零刚度隔振器进行模态仿真、谐响应仿真及随机振动仿真。仿真结果表明，准零刚度隔振器相较于线性隔振器具有更小的初始隔振频率，更大的隔振范围，峰值振动隔振可达到 11.58 dB。

关键词：隔振；准零刚度；屈曲；欧拉梁；有限元分析